JOURNAL OF GEOPHYSICAL RESEARCH, VOL. 99, NO. C8, PAGES 16,293–16,301, AUGUST 15, 1994

On the statistics of the phase of microwave backscatter from the ocean surface

R. D. Chapman, B. L. Gotwols, and R. E. Sterner II
Applied Physics Laboratory, Johns Hopkins University, Laurel, Maryland

Abstract. In this paper we describe what we believe is the first study of the distribution of the phase of microwave fields backscattered from the ocean surface. Scatterometry data from the Synthetic Aperture Radar and X band Ocean Nonlinearities experiment conducted on the German North Sea Research Platform, Forschungsplatform Nordsee, in November 1990 have been analyzed to reveal the distribution of phase differences as a function of time lag. A theoretical model for these statistics is presented based on modulated Gaussian fields. This theoretical model is shown to be in good agreement with the measured statistics. From this agreement we conclude that the backscattered fields have a Gaussian distribution on short time scales but are modulated in amplitude and frequency by the long surface waves. These results are of more than purely academic interest, with direct applications to the design and analysis of interferometric synthetic aperture radars, a relatively new class of instruments that may be capable of providing high-resolution maps of ocean surface currents from aircraft or satellites.

Introduction

Microwave backscatter from the ocean surface at moderate incidence angles has been investigated in numerous studies. Most of these studies have been limited to measurement of the mean backscatter power and its dependence on environmental parameters [e.g., *Jones and Schroeder*, 1978]. A few studies have reported on the first-order statistics of the amplitude or power of the backscattered field and their dependence on environmental parameters [*Trizna*, 1991; *Gotwols and Thompson*, 1994]. These first-order statistics are applicable to wind measurements using scatterometers and surface wave and current feature measurements using synthetic aperture radars (SAR), as well as to a wide range of problems involving the detection of targets in the presence of sea clutter.

A second, smaller class of studies has examined the spectrum of the backscattered field [e.g., *Plant and Keller*, 1990]. The purpose of most of these studies has been to examine the details of the scattering mechanism. The principal application of such studies has been to SAR imaging theory.

Another class of statistical studies has examined the joint statistics of radar backscatter parameters. Examples include modulation transfer function studies which look at the coherence of the mean Doppler frequency with the amplitude of the return [*Plant*, 1989]. This has direct applications to SAR imaging theory. Other joint statistics studies have characterized the correlation of near-nadir backscattered power and wave height to examine the electromagnetic bias that affects radar altimeters [*Melville et al.*, 1991].

None of the studies that we are aware of has presented measurements of the statistics of the phase of the backscattered field, the topic of this paper. This study is of more than academic interest. The backscatter phase fluctuations provide an underlying noise floor for a relatively new class of remote sensors, called along-track interferometric synthetic aperture radars (INSAR) [*Goldstein and Zebker*, 1987; *Goldstein et al.*, 1989]. The INSAR provides a promise of measuring ocean currents directly from aircraft or satellites [*Thompson and Jensen*, 1993; *Shemer et al.*, 1993]. Its operation depends on making measurements of the difference in backscatter phase at two separate times. Thus the statistics of phase fluctuations are a necessary component in any model of INSAR performance.

This study has been limited to data and models pertinent to moderate incidence angle backscatter, angles from approximately 30° to 60°. Hence the model developed here may not be applicable to normal incidence or near-grazing angle measurements.

Copyright 1994 by the American Geophysical Union.

Paper number 94JC01111.
0148-0227/94/94JC-01111$05.00

Theory

Consider an ideal continuous wave scatterometer viewing the ocean surface at a particular frequency f and incidence angle θ_i. The output of this device is a complex time series, $z(t) = I(t) + iQ(t) = a(t) \exp [i\phi(t)]$, where $I(t)$ and $Q(t)$ are the in-phase and quadrature components of the backscattered field, $a(t)$ is the amplitude, and $\phi(t)$ is the phase. The two representations of the field are related in the usual way: $a = (I^2 + Q^2)^{1/2}$ and $\phi = \tan^{-1} (I/Q)$. To a good first approximation we can treat the I and Q signals as being joint Gaussian random variables over short time scales [*Gotwols and Thompson*, 1994] with an autocovariance function given by $R(\tau) = \langle z(t) z^*(t + \tau) \rangle$. In the case of ocean backscatter the I and Q signals are not linearly correlated so that the phase $\phi(t)$ is a uniformly distributed random variable lying between 0 and 2π. More interesting are the differences in phase measured at two different times, $\Delta\phi(t; t + \tau) = \arg [z(t) z^*(t + \tau)]$, and in particular, the distribution of these phase differences. If the field is ergodic, then this distribution is only a function of the lag τ.

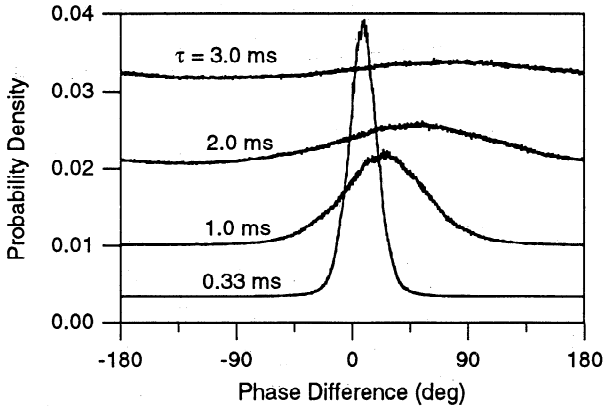

Figure 1. Probability density function for phase differences of a K_a band vertically polarized scatterometer for time lags of 0.33, 1.0, 2.0, and 3.0 ms. Each curve has been offset vertically an amount proportional to the temporal lag in order to separate the curves.

For a joint Gaussian distribution of I and Q, *Middleton* [1960, equation 9.32, p. 404] shows that the probability density function (pdf) of the phase differences, $p(\Delta\phi, \tau)$, can be expressed in terms of the autocorrelation function of the complex process $\rho(\tau)$:

$$p(\Delta\phi, \tau) = \frac{1 - |\rho|^2}{2\pi} (1 - \beta^2)^{-3/2}[\beta \sin^{-1} \beta + \frac{\pi\beta}{2} + (1 - \beta^2)^{1/2}] \quad (1)$$

where

$$\beta \equiv |\rho| \cos [\Delta\phi - \arg (\rho)]$$

and the autocorrelation function is given by the standard definition

$$\rho(\tau) = \frac{\langle z(t) z^*(t + \tau)\rangle}{\langle z(t) z^*(t)\rangle} \quad (2)$$

These expressions form the basis for our theoretical predictions, although as will be shown later, some modification of (2) is necessary to obtain good agreement between theory and measurements.

Measurements

The statistics of backscatter phase differences were estimated from scatterometer measurements obtained during the Syntheic Aperture Radar X band Ocean Nonlinearities–Forschungsplatform Nordsee (SAXON FPN) experiment. This joint German–United States experiment was conducted during the month of November 1990 from the German FPN tower located in the North Sea. The purpose of this experiment was to examine the mechanisms involved in the radar imaging of large ocean waves.

The principal measurement systems were an extensive set of coherent scatterometers and radars along with a variety of environmental measurement systems, all deployed on or about the FPN tower. In this study we made use of scatterometer data at five different wavelengths: L band (19.0 cm), S band (11.2 cm), X band (3.0 cm), K_u band (2.1 cm), and K_a band (0.86 cm). All of these instruments were operated at moderate incidence angles, typically 45°. The month long duration of the experiment allowed us to examine a wide range of environmental conditions. Supporting wind and wave measurements are presented for the data sets examined here. The reader is referred to *Plant and Alpers* [1994] for a more complete description of the SAXON FPN experiment and to *Thompson and Gotwols* [1994] and *Gotwols and Thompson* [1994] for a study of the amplitude statistics of the same scatterometer data analyzed in this paper.

To examine the distribution of phase differences in the backscattered signals as a function of temporal lag, all of the scatterometer data were analyzed in a similar manner. The complex backscatter time series were divided first into 5-min segments. A circularity correction was applied which compensates for mean amplitude and phase differences between the in-phase (I) and quadrature (Q) channels.

The phase statistics for these data were estimated by computing histograms of the phase differences over various temporal lags defined by

$$\Delta\phi = \arg (z(t) z^*(t + \tau)) \quad (3)$$

Normalization of the histogram results in an estimate for the probability of occurrence of a given phase lag given a specified time lag $p(\Delta\phi; \tau)$. This is the statistical measure of the phase differences which we compare with theory.

Figure 1 shows four such pdf estimates made for time lags of 0.33, 1.0, 2.0, and 3.0 ms from 5 min of data from the K_a band vertically polarized scatterometer. These data were acquired at 0231 UTC on November 28, 1990. The winds on this day were coming from 34° at 4.8 m/s, as projected to a height of 19.5 m under neutral stability conditions. The radar was looking due north, so the waves were predominantly toward the radar. A swell of 17 cm rms amplitude from 323° was present, as measured by a nearby roll-pitch buoy.

At zero time lag we expect that there will be no phase differences, so the pdf in this limiting case should be a delta function (not shown in Figure 1). The pdf for the shortest available time lag of 0.33 ms is narrowly distributed about a mean phase difference of about 8°. At a time lag of 1 ms the pdf has broadened considerably, with a mean of about 24°. A linear relationship between mean phase difference and time lag exists until the phase decorrelates to the point where it wraps around onto itself. In the limit of long lag time we expect that the scattered field will decorrelate and the phase differences will be uniformly distributed between −180° and +180° with a mean phase of 0°. The decorrelation of the phase differences at 3-ms time lag is evident in Figure 1.

The linear relationship between mean phase difference and time lag corresponds to a mean positive Doppler shift due to the surface scatterers moving toward the radar. A mean scatterer "velocity," actually the mean velocity of the scattering phase center, can be estimated from the slope of this relationship.

An alternative contour representation of the same pdf estimates is shown in Figure 2. This figure was created by computing the pdf over a rectilinear grid of phase differences and temporal lags and then contouring the resulting array. We have cut off the data at the shortest nonzero lag supported by the 3-kHz sampling rate used in this experiment. This cutoff was applied specifically to avoid the

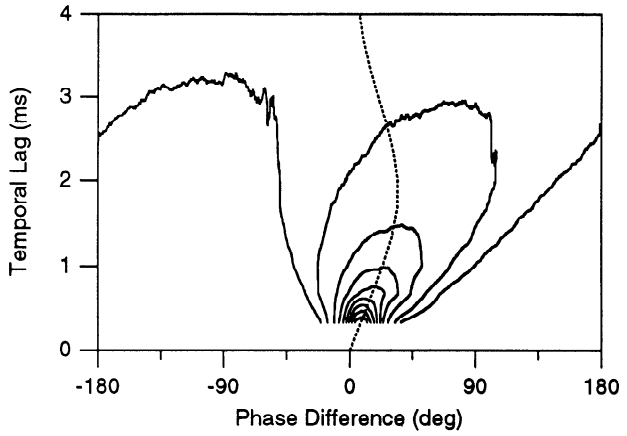

Figure 2. Contour plot of probability density function for phase differences of a K_a band scatterometer as a function of time lag. The probability contours occur at values of 0.002, 0.004, 0.008, 0.012, 0.016, 0.020, 0.024, 0.028, and 0.032, with the smallest probability densities occurring at the largest phase differences. The dotted curve is a plot of the mean phase difference versus temporal lag. The linearity of this relationship for short lag times is evident.

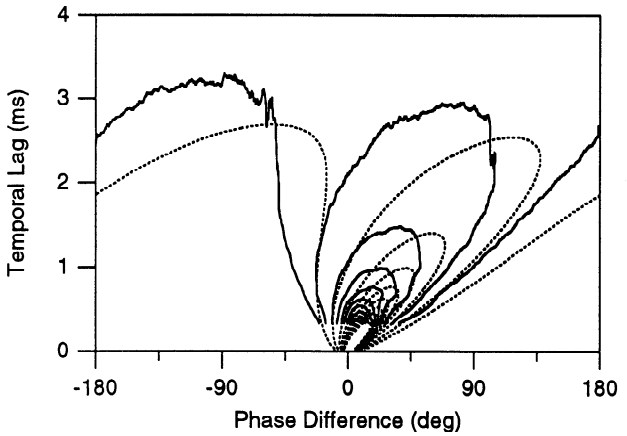

Figure 3. Comparison of theoretical (dashed) and measured (solid) K_a band vertically polarized phase difference pdf. The theoretical curve is derived from the standard theory of Gaussian-distributed fields.

difficulties associated with drawing contours about a delta function.

Similar phase difference pdf estimates were computed from the other scatterometer data taken during the same 5-min time period. The estimated phase difference decorrelation times (the times for the peak in the autocorrelation of the phase difference to fall below 0.004) are listed in Table 1. The backscatter phase decorrelates due to a combination of the random motions and finite lifetimes of the surface scatterers [*Plant*, 1991]. *Plant et al.* [1994] have shown that the correlation times at X and K_a bands can be accurately estimated from measurements of the rms surface velocities within the radar footprint using a relatively simple model. The decorrelation times measured here are not directly comparable to the more standard correlation time, except in the limit of Gaussian statistics, but it is interesting to note that the correlation times at X and K_a bands reported by *Plant et al.* [1994] are comparable to the decorrelation times measured here.

Comparison of Theory and Measurements

We have presented a simple theory and measurements describing the first-order statistics of phase differences for microwave energy backscattered from the ocean surface. In this section we compare theory and measurements, showing that there are substantial discrepancies between the two. We then describe the physical mechanisms for these discrepancies and present an amended theory with substantially better agreement.

Table 1. Estimated Phase Difference Decorrelation Time as a Function of Radar Frequency

Band	Frequency, GHz	Decorrelation Time, ms
K_a	35.000	3
K_u	14.000	7
X	10.000	10
S	2.671	35
L	1.579	58

Comparison With Theory for Gaussian-Distributed Fields

Figure 3 shows a comparison of the standard theory for joint Gaussian-distributed fields (equation (1)) with the measured data, corresponding to the 5-min data set in Figures 1 and 2. The theoretical curves were computed by estimating the complex autocorrelation function from the 5 min of data using (2) and substituting the result into Middleton's equation (1). While the general character of the curves is similar, there are also substantial differences: the measured decorrelation times are slightly longer than predicted, the width of the measured pdf is slightly greater than predicted, and the mean phase difference is overpredicted for each lag. The implications of this latter observation are particularly important for INSAR measurements, as it suggests a mechanism for error in estimating surface currents from remote phase difference measurements. Similar discrepancies have been observed at the other wavelengths, although the discrepancy in the mean phase difference is smaller at L band than at K_a band.

Non-Gaussian Surface Mechanisms

This discrepancy between the simple theory of joint Gaussian-distributed fields and the measurements can be explained in terms of the correlation of amplitude and frequency modulations of the ocean scatterers. The physical picture is a simple one. It has been shown that microwave backscatter at moderate incidence angles is dominated by Bragg scattering [*Plant and Keller*, 1990]. The returns from these small-scale surface scatterers are subjected to both amplitude and frequency modulations. The amplitude modulations in the scattered field are due to hydrodynamic modulation of the Bragg scatterer amplitudes as well as tilt modulation, where the local Bragg condition varies with the local mean tilt of the surface causing an apparent modulation in the Bragg scatterer amplitudes. At the same time the Bragg scatterers are being advected toward and away from the radar by the orbital currents of longer gravity waves.

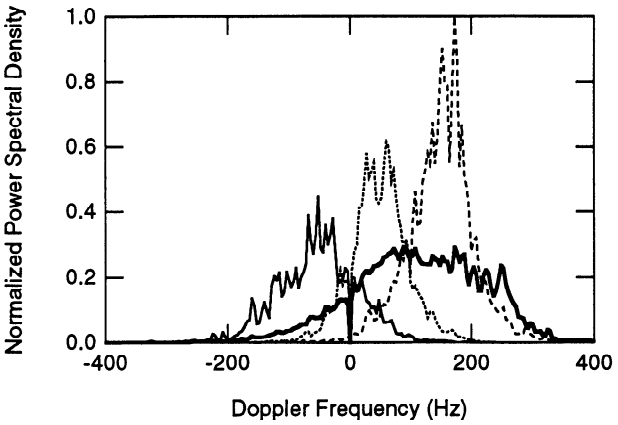

Figure 4. Doppler spectra conditionally sampled on the mean Doppler frequency. The thin solid, dotted, and dashed curves are an average of those spectra whose mean Doppler frequencies lie within ±10 Hz of −50, +50, and +150 Hz, respectively. The thick solid curve is the mean Doppler spectrum for the entire 5-min period. The correlation of frequency and amplitude modulations are clearly apparent in the conditionally sampled spectra, with the high-frequency spectra having larger amplitude than the low-frequency spectra. The notch at 0 Hz is an instrumental effect.

This advection causes frequency modulation of the Bragg scattering peaks.

The frequency and amplitude modulations of the Bragg scatterers are in fact coherent, as measured by the classic Modulation Transfer Function (MTF) analysis pioneered by *Keller and Wright* [1975]. The correlation of these modulations can be seen in the scatterometer data by conditionally averaging short time Doppler spectra based on their mean Doppler frequency. In particular, the time series is broken into 0.25-s segments, which is short compared to the dominant wave period of 6.7 s but long with respect to the measured backscatter power decorrelation time of 10 ms, as measured at K_a band. A 2 degree of freedom Doppler spectrum estimate is made from each of these segments along with a mean Doppler frequency estimate. In particular, for each 0.25-s segment of data we compute $\Phi(f) = |\int h(t)z(t)e^{i2\pi ft}\,dt|^2$, where $h(t)$ is a Hanning window. From this spectral estimate we derive an estimate for the short term mean Doppler frequency from $\bar{f}_d = \int f\Phi(f)\,df / \int \Phi(f)\,df$. All of the Doppler spectra whose mean Doppler frequency fell within a specified range were then averaged together. Figure 4 presents the results of such a calculation.

The correlation of the frequency and amplitude modulations is quite apparent in Figure 4. The spectra which peak at high frequencies have larger amplitudes than the low-frequency spectra. This correlation tends to bias long-term estimates of mean frequency to higher values, as the higher-frequency components are weighted more heavily than the lower-frequency components.

The reason for the discrepancies in the predicted and measured phase difference statistics arises from this simple physical model. The phase statistics are insensitive to any variations in amplitude, at least as long as the signals are above the system noise floor. In contrast, the simple Gaussian theory depends on estimates of the autocorrelation function of the field which are sensitive to amplitude variations. In particular, the autocorrelation function is biased toward decorrelation at shorter lags due to the same mechanism that biases the Doppler spectrum. Thus we were motivated to remove the amplitude modulations from the autocorrelation estimates used to predict the phase difference distributions.

Comparison With Normalized Gaussian Theory

Equation (4) is an expression for a normalized autocorrelation function estimate $\rho'(\tau)$ that removes the effect of amplitude variations:

$$\rho'(\tau) = \left\langle \frac{\langle z(t)z^*(t+\tau)\rangle|_{0.25s}}{\langle z(t)z^*(t)\rangle|_{0.25s}} \right\rangle \tag{4}$$

where the notation $\langle\ \rangle|_{0.25s}$ means average over 0.25-s time intervals and angle brackets mean average over all measurements. To evaluate (4) we broke the 5-min data record into 1200 individual 0.25-s segments, computed an autocorrelation function estimate for each segment, and then averaged all of these estimates together to obtain a single normalized autocorrelation estimate for the entire time series. This initial averaging over 0.25-s intervals removes the influence of amplitude variations occurring on time scales longer than 0.25 s. This estimator was used with (1) to compute an improved prediction for the distribution of phase differences. The results, shown in Figure 5, agree quite well with the measured values.

The same calculations have been performed at all of the other available wavelengths and polarizations (Figure 6). Similar levels of agreement are observed. We have performed similar calculations with data from another time period during the SAXON FPN experiment (with higher wind speeds of 9.9 m/s) and for some K_u band data taken during the 1988 SAXON experiment at the Chesapeake Light Tower. (The details of the environmental conditions during these three periods are given by *Gotwols and Thompson* [1994].) Again the agreement is quite good in all of the cases we examined.

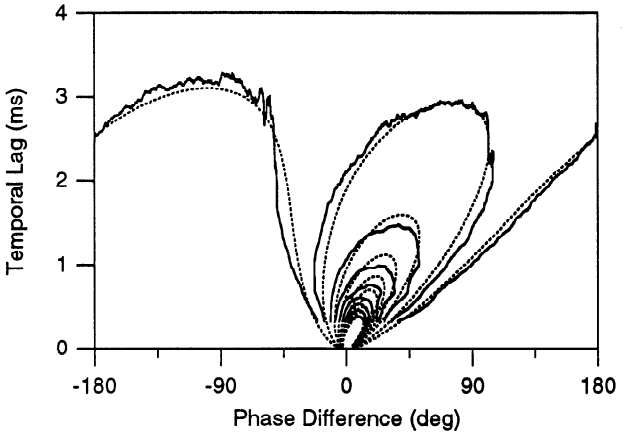

Figure 5. Comparison of improved theoretical (dashed) and measured (solid) K_a band vertically polarized phase difference pdf. The theoretical curve is derived from the theory for a joint Gaussian-distributed field with a normalized autocorrelation estimate which removes the effects of slow amplitude modulations due to long waves. This improved theory agrees with measurements significantly better than the simple theory shown in Figure 3.

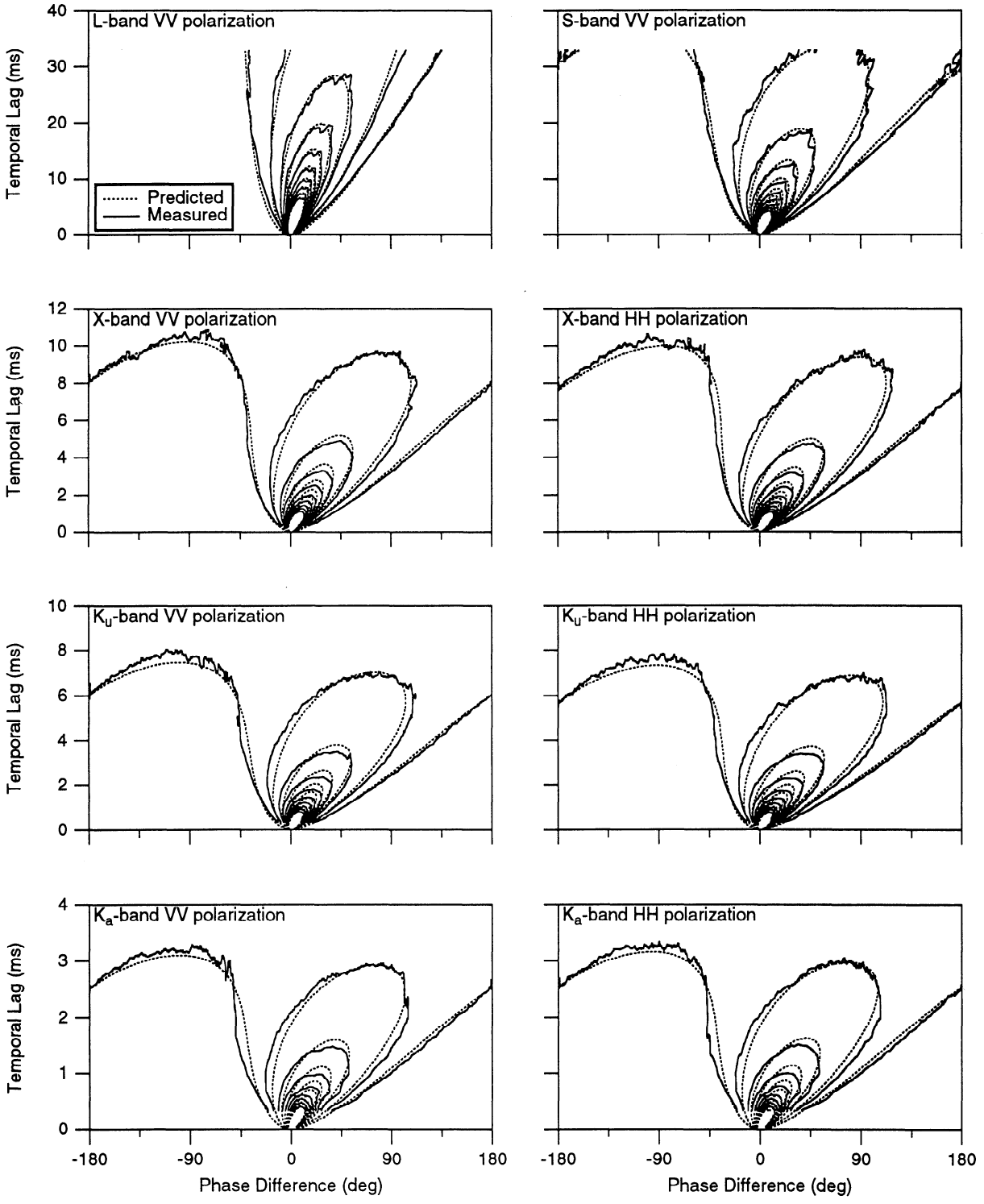

Figure 6. Comparison of improved theoretical (dotted) and measured (solid) phase difference pdf for all wavelengths and polarizations. While these data were obtained under a uniform set of environmental conditions (wind speed of 4.8 m/s at a height of 19.5 m), similar levels of agreement have been obtained for other data sets obtained under different environmental conditions.

The reader is cautioned, however, that we have restricted our studies to portions of the data set where the waves were propagating mostly into the look direction of the scatterometers. Other data were ignored due to the possible contamination of the wind field by the tower and reflections of surface waves from the tower legs. The accuracy of applying this theory to the case of cross-wind illumination direction is not known, although we foresee no mechanism that would reduce the accuracy in these cases.

Discussion

A simple theory has been presented that accurately predicts the distribution of phase differences of microwave backscatter at moderate incidence angles. This theory works surprisingly well at all five wavelengths studied: L, S, X, K_u, and K_a bands and under a variety of conditions where the surface waves were propagating toward the radar look direction. The theory is based on a modification of Middleton's formula for the distribution of phase differences as a function of time lag for a jointly Gaussian distributed process. This modification removes the amplitude variations that occur in the backscattered signal due to the tilting and modulation of the local scatterers by long waves.

Gotwols and Thompson [1994] used a similar technique for removal of long wave-induced amplitude modulations to show that the backscatter amplitude is Rayleigh distributed over time scales short with respect to the long wave periods. A Rayleigh distribution of amplitude arises directly from a joint Gaussian distribution of the field. In this study we have shown that over similarly short time scales the distribution of the phase differences corresponds to that predicted for a Gaussian field. Thus we can conclude that the full complex backscattered field is essentially joint Gaussian distributed over time scales short with respect to the periods of the long waves.

The 0.25-s time scale used in this study was chosen specifically to be short with respect to the long wave period but long with respect to the phase decorrelation time. While the effects described in this work could have been illustrated with 0.1- to 0.5-s averages, it is interesting to consider the question of how long can one wait before the distributions become significantly non-Gaussian. In general, the answer is dependent on the amplitude and frequency of the modulating long waves. Note that this does not necessarily correspond to the dominant wave associated with a peak in the wave height spectrum. The amplitude modulations are principally correlated with the local surface slope, and the frequency modulations are correlated with the orbital velocity of the long waves. The peaks in the spectra of slope and orbital velocity occur at higher frequencies than the peak in the wave amplitude. Thus the modulations occur at shorter time scales than one might initially expect from the wave height spectrum.

Applications to Interferometry

The canonical along-track interferometric synthetic aperture radar consists of two separate synthetic aperture radars mounted on the same platform with antennas separated in the along-track dimension. Actual systems typically consist of a single transmitter and a pair of receivers and receive antennas, but the operation of such a system is most easily understood in terms of two separate SARs. One additional requirement for such a system is that the two SARs must be phase coherent over the time scales used to form the image.

In the first step of INSAR processing, returns from each of the two SARs are processed to form two separate complex radar backscatter images. These images are then coregistered such that each covers the same area on the ground. The image from the trailing SAR is formed at time $\Delta t = D/V$ after the formation of the leading SAR image, where D is the distance between the antennas and V is the velocity of the INSAR platform. The phase difference between the two images is then calculated pixel by pixel to provide the interferometric estimate of the scatterer velocities observed throughout the imaged swath.

Ignoring the complexities of the SAR image formation mechanisms, it is apparent that the INSAR measurement of phase differences is identical to the process examined in this paper using scatterometer data. This correspondence holds as long as the actual scatterer velocity is less than the INSAR ambiguity velocity, that is, the radial velocity at which a scatterer must move for the SAR to misregister the location of that scatterer by exactly one half pixel in azimuth. Thus the statistics of the phase differences that we have presented here also apply to the phase differences observed with an INSAR. There are several implications of this observation.

Noise floor. The fundamental noise floor of an INSAR system is set by the phase difference fluctuations examined in this paper. Given a system with an infinite signal-to-noise ratio (which turns out to be very expensive to build!), the accuracy with which the mean phase difference can be computed depends on the width of the distributions described by (1) and (4).

Antenna separation distance. The optimum along-track antenna separation distance, a key INSAR design parameter, is dependent on the backscatter phase statistics. To see this, imagine an INSAR with an antenna separation and platform velocity such that the time lag between the formation of the leading and trailing images was greater than the phase decorrelation time. In this case the phases in the two images would be uncorrelated, and the interferometer would provide no useful information. Phase correlation increases with decreasing temporal lag, suggesting that the antenna separation should be as small as possible. On the other hand, the mean phase difference also decreases as the antenna separation decreases. The minimum detectable mean phase difference is typically set by receiver noise characteristics. Thus the optimal separation of antennas is set by a balance between the decorrelation of the backscattered phase and receiver phase noise.

Phase difference estimator. The phase difference estimator used in INSAR processing can be formed in one of several ways. Two estimators that have been used in existing INSAR systems are $\arg [\langle z(t) z^*(t + \tau)\rangle]$ and $\langle \arg [z(t) z^*(t + \tau)]\rangle$. These two forms are not equivalent, that is, the phase of the means is not equal to the mean of the phases. The former estimator is biased by any correlations of amplitude and phase modulations, just as in the example of Figure 4. The latter estimator, which is amplitude independent, is an optimal estimator for the mean phase difference.

The bias introduced by use of the first estimator is illustrated in Figure 7. The mean Doppler frequency derived from the standard Doppler spectrum (solid line) is 113 Hz. An optimal scatterer velocity estimate would be uninflu-

enced by amplitude variations within the signal, so we computed a normalized Doppler spectrum from the Fourier transform of the normalized autocorrelation function given in (4) multiplied by the variance of the entire time series. It is easy to show that this normalized Doppler spectrum is equivalent to the spectrum of the time series with the amplitude variations removed. In addition, it is interesting to note that according to Woodward's theorem this normalized spectrum asymptotically approaches the form of the short time lag phase difference pdf in the limit of slow frequency modulations [*Blachman and McAlpine*, 1969]. The center frequency of this normalized spectrum is 70 Hz. Thus in this example an INSAR-derived current estimate would be in error by a factor of 60% if the INSAR phase was based on a 5-min average using the biased phase difference estimator.

Realistic INSAR systems have integration times from a few tenths of a second to a few tens of seconds. The degree of bias in such a system would depend on the actual integration time and the amplitude and wave period of the dominant modulating long waves. For example, a reduction of the integration time to 5 s in the above example shifts the mean frequency of the biased estimator to approximately 90 Hz. This effect is illustrated by comparing various mean frequency estimators as a function of the temporal length of the processing window (Figure 8).

There are three mean frequency estimators shown in Figure 8. The mean Doppler frequency estimate is computed from an ensemble average of spectra computed from sections of the data with the specified window length. Thus the mean Doppler frequency estimate for a 10-s window is based on the mean frequency of an ensemble average of 30 spectra, each computed from 10 s of data. The mean normalized Doppler frequency estimate is computed by normalizing each member spectrum from the ensemble to unity power prior to performing the ensemble average. This has the effect of removing amplitude fluctuations longer than the time scale of the processing window. The final estimator, which we refer to as the normalized data frequency estimator, is a pure phase-based estimate made by normalizing each individual complex sample in the 5-min time series to unit amplitude prior to computation of the mean Doppler frequency.

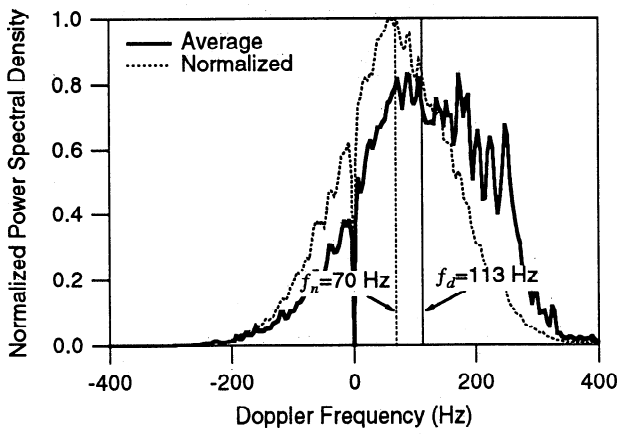

Figure 7. Doppler spectrum for 5 min of K_a band data (solid curve) and the normalized Doppler spectrum (dashed curve) formed from the Fourier transform of the normalized autocorrelation given in (4) multiplied by the variance of the entire time series. The mean frequency of the normalized Doppler spectra (70 Hz) is an optimum estimate of the mean phase velocity of the scattered field. In contrast, the mean Doppler frequency (113 Hz) is a biased estimator with added weight given to higher-amplitude portions of the signal.

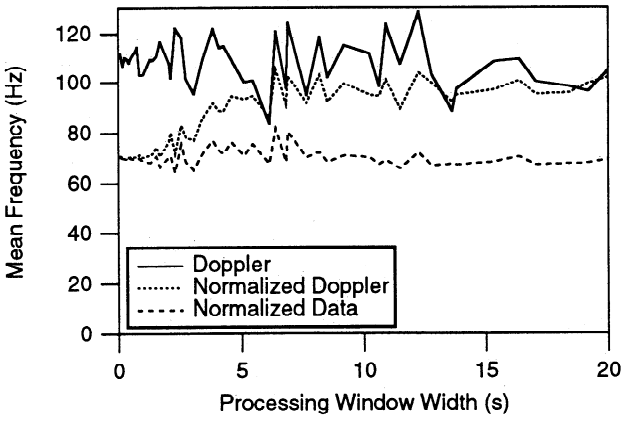

Figure 8. Three mean frequency estimates as a function of the temporal length of the processing window. The Doppler estimator is always biased high. The normalized Doppler estimator varies between the normalized data estimator at short times to the Doppler estimator at long times.

The mean Doppler and normalized data estimators are relatively insensitive to the windowing time, although the mean Doppler estimates are biased high (for approaching waves) due to the correlation of amplitude and frequency modulations. The noise in the mean Doppler estimator can be associated with the amplitude fluctuations in the time series which are not present in the normalized data estimator. The normalized Doppler frequency varies from agreement with the normalized data estimate for short time windows to the mean Doppler estimate for long time windows. In this particular case, processing times would have to be kept to less than 2 s (25% of the long wave period) in order for the frequency estimator to be within 10% of the unbiased value. Given this sensitivity, INSAR phase differences should be estimated using the unbiased estimator.

Spectral Width. The width of the phase difference distribution is proportional to the noise in the mean phase estimate. This width is in turn dependent on the width of the normalized Doppler spectrum. In Figure 4 it is clear that the long time average Doppler spectrum is wider than the short-term Doppler spectrum. A crude estimate of the relative widths shows a factor of 3 difference in this example. The frequency modulation of the short-term signals is thus responsible for a major portion of the width of the spectra. We expect that this same broadening of the Doppler spectrum occurs on short time scales if the scatterometer footprint is increased to dimensions approaching those of the long waves. From this observation we conclude that a high-resolution, short-dwell time INSAR would have lower per pixel phase noise than a system with either low-resolution or long-dwell time. (In this case the qualifiers long and short are determined from comparison with the period and wavelengths of the dominant modulating waves.) This is directly related to the previous point, in that we suggest that the phases be determined first and then averaged together, and not the other way around.

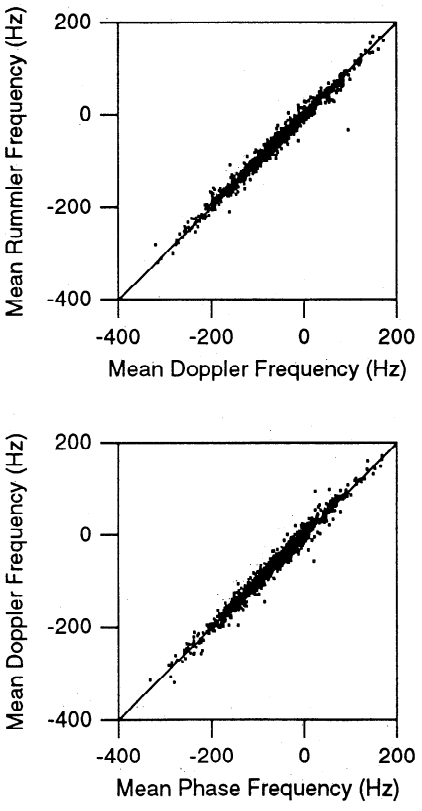

Figure 9. Comparisons of three different methods of estimating mean frequencies. Shown are the mean Doppler frequency $\bar{f}_d$, the Rummler estimator $\bar{f}_r$, and the mean phase estimator $\bar{f}_p$, evaluated for $\tau = 333$ μs. If the estimators were in perfect agreement, all of the points would lie along the thin solid reference line.

Applications to MTF Analysis

In the mid 1970s the concept of MTF analysis was introduced [*Keller and Wright*, 1975] to provide a means of estimating the hydrodynamic modulation of scatterers by long waves for use in SAR imaging theories. This technique involves several steps. First, time series of power and mean Doppler frequency are derived from the complex backscattered signal. The mean Doppler frequency is then associated with the radial velocity of the scatterers along the radar line of sight. Application of simple wave dynamics allows the velocity time series to be transformed into a slope time series, at least for each frequency component of the long waves. Switching into the spectral domain, where the coherence of the slope and power are then computed, provides information on the relative modulation of the scatterers by different long wave spectral components.

We have discussed the biases that exist in phase velocity estimators derived from mean Doppler frequencies. The question naturally arises as to whether the frequency estimates commonly used in the MTF technique are biased. We believe that the bias is negligible as long as estimates of the mean frequency and power are made over time intervals that are short with respect to the period of the modulating waves. Thus the amplitude varies little during the estimation period, typically 0.1 to 0.4 s, and so the mean Doppler frequency is unbiased. To demonstrate this we computed time series of the mean frequency for the sample data set using three distinct estimators. Each estimator was applied to 0.25-s intervals of data, and comparisons were made to examine any differences between the three methods. The first estimator was the mean Doppler frequency, defined by $\bar{f}_d = \int f\Phi(f)\, df / \int \Phi(f)\, df$, where $\Phi(f)$ is the short-term Doppler spectrum. The second method is the Rummler estimator given by $\bar{f}_r = (2\pi\tau)^{-1} \arg [\langle z(t)z^*(t + \tau)\rangle]$, where τ is taken to be as small as possible. *Miller and Rochwarger* [1972] show that this estimator converges to the mean Doppler frequency for short lag times. Finally, we computed a mean phase estimator, defined by $\bar{f}_p = (2\pi\tau)^{-1}\langle \arg [z(t)z^*(t + \tau)]\rangle$. The mean phase estimator is taken as the true value of the mean phase difference.

A comparison of the values derived using these three estimators for $\tau = 333$ μs is presented in Figure 9. It is evident that all of these estimators agree quite well, and any errors due to estimator bias on these short time scales must be small.

Acknowledgments. We would like to thank all of our SAXON collaborators. In particular, the primary data presented in this paper were obtained from scatterometers deployed by Bill Plant, Gene Terray, and Bob Petit of the Woods Hole Oceanographic Institution (X and K_a band), Bill Keller of the Naval Research Laboratory (L and S band), and Ken Melville and David Arnold of the Massachusetts Institute of Technology (K_u band). Siegfried Stolte of the Forschungsanstalt der Bundeswehr für Wasserschall- und Geophysik (Kiel, Germany) provided the meteorological data and Friedwart Ziemer of the Forschungszentrum Geesthacht GmbH (Geesthacht, Germany) provided directional wave spectra derived from a roll-pitch buoy. We'd also like to thank Gene Terray for his insights into the intricacies of Doppler frequency estimation. United States participation in the SAXON FPN experiment and this work were sponsored by Frank Herr and Dennis Trizna of the Office of Naval Research.

References

Blachman, N. M., and G. A. McAlpine, The spectrum of a high-index FM waveform: Woodward's theorem revisited, *IEEE Trans. Commun. Technol., COM-17*(2), 201–207, 1969.

Goldstein, R. M., and H. A. Zebker, Interferometric radar measurement of ocean currents, *Nature, 328*, 707–709, 1987.

Goldstein, R. M., T. P. Barnett, and H. A. Zebker, Remote sensing of ocean currents, *Science, 246*, 1282–1285, 1989.

Gotwols, B. L., and D. R. Thompson, Ocean microwave backscatter distributions, *J. Geophys. Res., 99*, 9741–9750, 1994.

Jones, W. L., and L. C. Schroeder, Radar backscatter from the ocean: Dependence on surface friction velocity, *Boundary Layer Meteorol., 13*, 133–149, 1978.

Keller, W. C., and J. W. Wright, Microwave scattering and the straining of wind-generated waves, *Radio Sci., 10*, 139–147, 1975.

Melville, W., R. Stewart, W. Keller, J. Kong, D. Arnold, A. Jessup, M. Loewen, and A. Slinn, Measurement of electromagnetic bias in radar altimetry, *J. Geophys. Res., 96*(C3), 4915–4924, 1991.

Middleton, D., *An Introduction to Statistical Communications Theory*, McGraw-Hill, New York, 1960.

Miller, K. S., and M. M. Rochwarger, A covariance approach to spectral moment estimation, *IEEE Trans. Inf. Theory, IT-8*(5), 588–596, 1972.

Plant, W. J., The modulation transfer function: Concept and applications, in *Radar Scattering From Modulated Wind Waves*, edited by G. J. Komen and W. A. Oost, pp. 155–172, Kluwer Academic, Norwell, Mass., 1989.

Plant, W. J., The variance of the normalized radar cross section of the sea, *J. Geophys. Res., 96*, 20,643–20,654, 1991.

Plant, W. J., and W. Alpers, An introduction to SAXON-FPN, *J. Geophys. Res., 99*, 9699–9703, 1994.

Plant, W. J., and W. C. Keller, Evidence of Bragg scattering in microwave doppler spectra of sea return, *J. Geophys. Res., 95*(C9), 16,299–16,310, 1990.

Plant, W. J., E. A. Terray, R. A. Petitt Jr., and W. C. Keller, The

dependence of microwave backscatter from the sea on illuminated area: Correlation times and lengths, *J. Geophys. Res.*, *99*, 9705–9723, 1994.

Shemer, L., M. Marom, and D. Markam, Estimates of currents in the nearshore ocean region using interferometric synthetic aperture radar, *J. Geophys. Res.*, *98*(C4), 7001–7010, 1993.

Thompson, D. R., and B. L. Gotwols, Comparisons of model predictions for radar backscatter amplitude probability density functions with measurements from SAXON, *J. Geophys. Res.*, *99*, 9725–9739, 1994.

Thompson, D. R., and J. R. Jensen, Synthetic aperture radar interferometry applied to ship-generated internal waves in the 1989 Loch Linnhe experiment, *J. Geophys. Res.*, *98*(C6), 10,259–10,269, 1993.

Trizna, D. B., Statistics of low grazing angle radar sea scatter for moderate and fully developed ocean waves, *IEEE Trans. Antennas Propagation*, *39*(12), 1681–1690, 1991.

R. D. Chapman, B. L. Gotwols, and R. E. Sterner II, Applied Physics Laboratory, Johns Hopkins University, Johns Hopkins Road, Laurel, MD 20723.

(Received November 29, 1993; revised April 25, 1994; accepted April 25, 1994.)